AFRL-AFOSR-JP-TR-2023-0062

Interlayer Excitons as quantum emitters in 2D materials

Aharonovich, Igor
UNIVERSITY OF TECHNOLOGY SYDNEY
15 BROADWAY
ULTIMO, , 2007
AUS

02/28/2023
Final Technical Report

Air Force Research Laboratory
Air Force Office of Scientific Research
Asian Office of Aerospace Research and Development
Unit 45002, APO AP 96338-5002

REPORT DOCUMENTATION PAGE

PLEASE DO NOT RETURN YOUR FORM TO THE ABOVE ORGANIZATION.

1. REPORT DATE	2. REPORT TYPE	3. DATES COVERED	
20230228	Final	START DATE 20200504	END DATE 20220503

4. TITLE AND SUBTITLE
Interlayer Excitons as quantum emitters in 2D materials

5a. CONTRACT NUMBER	5b. GRANT NUMBER	5c. PROGRAM ELEMENT NUMBER
	FA2386-20-1-4014	61102F
5d. PROJECT NUMBER	**5e. TASK NUMBER**	**5f. WORK UNIT NUMBER**

6. AUTHOR(S)
Igor Aharonovich

7. PERFORMING ORGANIZATION NAME(S) AND ADDRESS(ES)
UNIVERSITY OF TECHNOLOGY SYDNEY
15 BROADWAY
ULTIMO 2007
AUS

8. PERFORMING ORGANIZATION REPORT NUMBER

9. SPONSORING/MONITORING AGENCY NAME(S) AND ADDRESS(ES)	10. SPONSOR/MONITOR'S ACRONYM(S)	11. SPONSOR/MONITOR'S REPORT NUMBER(S)
AOARD UNIT 45002 APO AP 96338-5002	AFRL/AFOSR IOA	AFRL-AFOSR-JP-TR-2023-0062

12. DISTRIBUTION/AVAILABILITY STATEMENT
A Distribution Unlimited: PB Public Release

13. SUPPLEMENTARY NOTES

14. ABSTRACT
This work investigated one the emerging field of interlayer excitons in 2D systems. These excitons form when two different monolayers are stuck together and have the potential to serve as sources of single photons that are required for most quantum applications, including unbreakable quantum cryptography. In addition, the project tackled issues of stability, synthesis and characterization of novel quantum emitters in 2D systems, to utilize them for quantum technologies and fundamental understanding of defects in 2D materials.

15. SUBJECT TERMS

16. SECURITY CLASSIFICATION OF:			17. LIMITATION OF ABSTRACT	18. NUMBER OF PAGES
a. REPORT U	b. ABSTRACT U	c. THIS PAGE U	SAR	7

19a. NAME OF RESPONSIBLE PERSON	19b. PHONE NUMBER *(Include area code)*
JEREMY KNOPP	315-227-7006

Standard Form 298 (Rev.5/2020)
Prescribed by ANSI Std. Z39.18

Final Report for AOARD Grant FA2386-20-1-4014

"Interlayer Excitons as quantum emitters in 2D materials"

Date 15/06/2022

Name of Principal Investigators (PI and Co-PIs): Igor Aharonovich, (UTS); Ruth Pachter (AFRL)

- e-mail address : igor.aharonovich@uts.edu.au
- Institution : University of Technology Sydney (UTS)
- Mailing Address : 15 Broadway, Ultimo, NSW 2007, Australia
- Phone : 95141702

Period of Performance: 05/01/2020 – 01/05/2022

Abstract: Two dimensional materials (2D) are the most prominent candidates for a new generation of devices in the fields of nanophotonics and nanoelectronics. This proposal investigated one the emerging field of interlayer excitons in 2D systems. These excitons form when two different monolayers are stuck together and have the potential to serve as sources of single photons that are required for most quantum applications, including unbreakable quantum cryptography. In addition, the project tackled issues of stability, synthesis and characterization of novel quantum emitters in 2D systems, to utilize them for quantum technologies and fundamental understanding of defects in 2D materials.

Introduction

Interlayer excitons (IEs) in van der Waals (vdW) heterostructures emerged as a promising platform for the studies of excitonic phenomena, many body physics, and optoelectronics. The IEs are constituted electron-hole pairs donated from adjacent monolayers, forming an indirect system with spatially separated but bound electron-hole pairs via Coulomb interactions (**Figure 1a**). When two monolayer transition metal di-chalcogenide (TMDCs) crystals are in close contact and form a type II band structure alignment, IEs will form due to the ultrafast charge transfer between the monolayers. As a result, the formation of the IEs would lead to a quench of the photoluminescence (PL) emission intensity of the individual monolayers. The emission energy from IEs is lower than the individual monolayers and the intensity is highly dependent on the stacking angles.

Here, we report on the integration of IEs from a heterostructures of tungsten di-sulphide and molybdenum di-sulphide (WS_2/MoS_2), into a nanoparticle-on-mirror plasmonic gap cavity. We demonstrate over an order of magnitude enhancement in PL intensity when IEs resonate with the plasmonic structures at room temperature. We further performed optical measurements at cryogenic temperatures (5 K) and observed a 5-times enhancement in PL intensity together with lifetime reduction in both fast and slow decay channels. The finite-difference time-domain (FDTD) simulation results reveal the enhancement of the emission is attributed to the higher excitation efficiency from the cavity accompanied with a Purcell enhancement. Our results present a novel approach to improve the excitonic processes in IEs from TMDCs heterojunctions and shed light on IEs based photonics and optoelectronic devices in near future.

Results and Discussions

We chose a nanoplasmonic gap cavity, consisting of a silver nanocube (~100 nm edge length) and an ultraflat gold mirror (~90 nm thickness). The resonance from these plasmonic gap cavities is broadband and thus is easily matched to the emission from IEs. It is expected that this type of cavities would enhance the emission from both in-plane and out-of-plane emitting dipoles by

accelerating the emission cycles (Purcell effect) and/or redirect the radiation pattern to favour collection. A schematic illustration of the nanogap cavity integrated IEs is presented in **Figure 1b**.

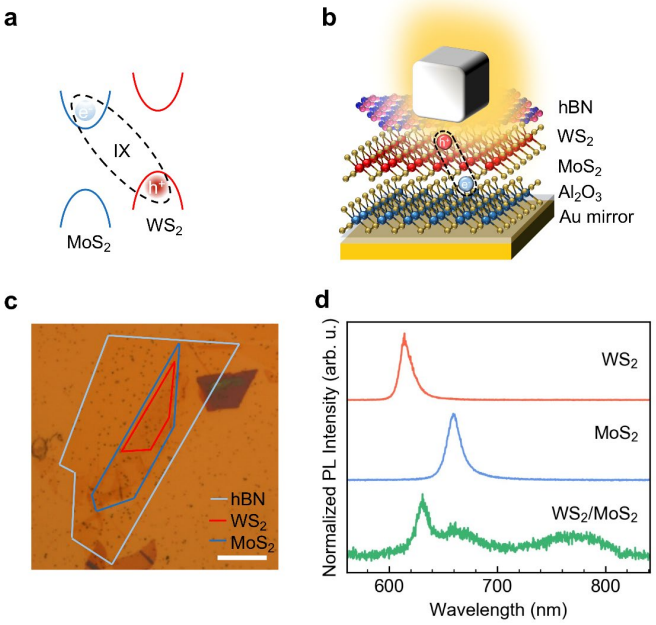

Figure 1. *(a) Schematic of the type II band alignment of a WS_2/MoS_2 heterostructure. (b) 3D illustration WS_2/MoS_2 heterostructure integrates with a plasmonic gap cavity. The gap cavity consists of a 100 nm silver nanocube and an ultra-flat gold film. The gold film is coated with 3nm thick Al_2O_3. A thin hBN flake is inserted as a space to tune the resonance wavelength to match the interlayer emission. (c) An optical image of the WS_2/MoS_2 heterostructure in the plasmonic cavity (scale bar: 5 μm), individual 2D flakes are outlined for clarity. (d) Normalized photoluminescence spectra of isolated monolayers WS_2 (red), MoS_2 (blue) and IEs (green, off cavity) at room temperature. The samples were excited with a 200 μW 532nm continuous wave laser.*

***Samples fabrication*:** A 90 nm thick ultraflat gold film is deposited onto a polished Si substrate using a slow-rate vacuum electron-beam deposition system. The gold surface is coated with a 3 nm thick Al_2O_3 layer using an atomic layer deposition system. Silver nanocubes (side length =100 nm) are purchased from Nanocomplex and the solution is diluted by 100 times using isopropanol prior to use.

Monolayer WS_2, MoS_2 and thin hBN flakes were mechanically exfoliated on silicon substrates with a 300 nm thermal oxide layer. The monolayers and the thickness of hBN flakes were identified firstly with optical microscopy followed by atomic force microscopy and photoluminescence, respectively. The heterostructures were stacked using a poly(vinyl alcohol) stamp based align transfer technique. The stamp was then dissolved with water to release heterostructures onto the gold ultraflat mirror. The silver nanocubes were drop-cast onto the heterostructures prior to optical measurements.

The silver nanocubes were diluted and dropped onto the heterostructures to form the nanogap modes. An optical microscope image is shown in **Figure 1c** with the individual crystals outlined in different colours (red: WS_2, blue: MoS_2 and grey: hBN) for clarity. The relative crystal orientation between WS_2 and MoS_2 were aligned with a precision ~ 1° along their longer edges. The PL spectra from monolayer WS_2, MoS_2 and IEs are plotted in Fig 1d.

***Photoluminescence spectroscopy*:** The PL spectra were collected with a home-built scanning confocal microscope. The samples were excited with a 200 μW 532nm continuous wave (CW)

laser. The reflection signal was spectrally filtered using a 532 nm dichroic mirror (LP03-532RE-25) and a 715 nm long pass filter. The time-correlated PL measurements were performed using the same setup where the samples were excited with a 20 μW 512 nm pulsed laser (PiL051X) with a repetition rate of 20 MHz. The laser signal and the PL from the samples (APD counts) were correlated using a time-correlated single photon counting system (PicoHarp 300). Low-temperatures optical measurements were conducted in the attoDRY800 cryostat.
The peaks centred at ~ 620 nm (red) and ~ 660 nm (blue) are associated with excitonic emission from WS_2 and MoS_2 monolayers, respectively. Some of the peaks rise at the longer wavelength are might be intralyer excitons and the formation are highly determined by multifactor, such as stacking angle, strain and materials combinations. The significantly reduced intensity from these two peaks together with the rise of the peak at ~ 780 nm indicates the successful formation of IEs according to the literature.

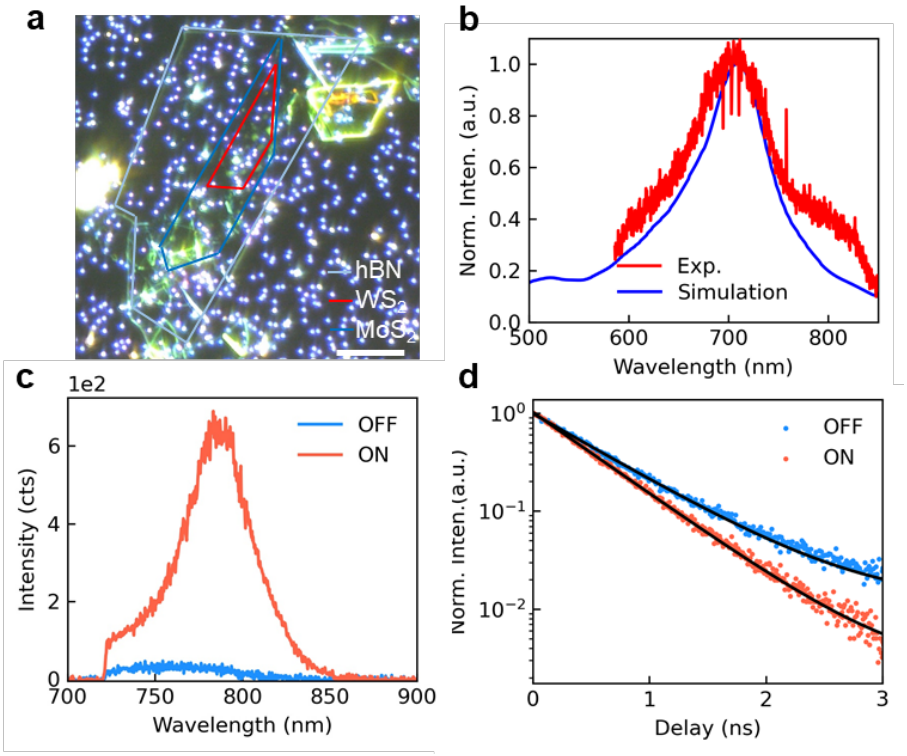

Figure 2. *(a) Dark-field image of corresponding overlapped region shown in Figure 1c. The 2D flakes are outlined and individual silver nanocubes are resolved. Scale bar: 5 μm. (b) Experimental and simulated optical scattering of a single nanocavity. (c) PL comparison between cavity coupling IE (red) and non-coupling IE (blue). (d) Time resolved PL of cavity coupled IE (red) and intrinsic IE (blue). The curves were fitted with a single exponential (black). The extracted lifetimes from fast decay are 526 ps and 652 ps, respectively.*

Systematic studies were performed to compare the emission of the IEs on and off plasmonic gap cavity. **Figure 2a** presents the dark-field image collected from the same sample region as shown in **Figure 1c**. The shining spots correspond to the silver nanocubes. There are ~15 cubes on top of the heterostructure regions, providing enough sample spots to compare the performance of the IEs coupled into cavities. The scattering spectra were collected from the cubes while shining halogen light on the sample with an incident angle of 28°. The normalised spectrum is shown in **Figure 2b**. The spectrum spans from 580 to 820 nm with a peak maximum centred at ~ 700 nm. The simulated scattering spectrum is also plotted which overlaps well with the experimental data. There is also a slight enhancement at ~532 nm which is not seen in the experimental results as it is blocked by our dichroic filter.
The PL spectra from the sample were then collected from the pristine IEs and cavity coupled

ones, as shown in **Figure 2c.** The PL from pristine IEs (red) shows maximum intensity at 765 nm, while the cavity-coupled IEs (blue) is red-shifted to ~780 nm, probably due to the cavity resonance. An overall ~ 15-times enhancement in peak height is observed, indicating that the plasmonic cavity has significantly enhanced the excitonic emission of IEs. Time-resolved PL (TRPL) measurements were then performed to understand the results. **Figure 2d** shows the TRPL measurements from pristine (red) and cavity coupled IEs (blue), as well as the instrument response function (IRF). The experimental decay curves were fitted using a double-exponential function. The lifetimes extracted from fast decay channels are 526 ps and 652 ps, respectively, corresponding to a measured reduction of 20%. The absolute lifetime values were longer than the ones reported before, probably because our samples have lower non-radiative decay rate at ambient conditions.

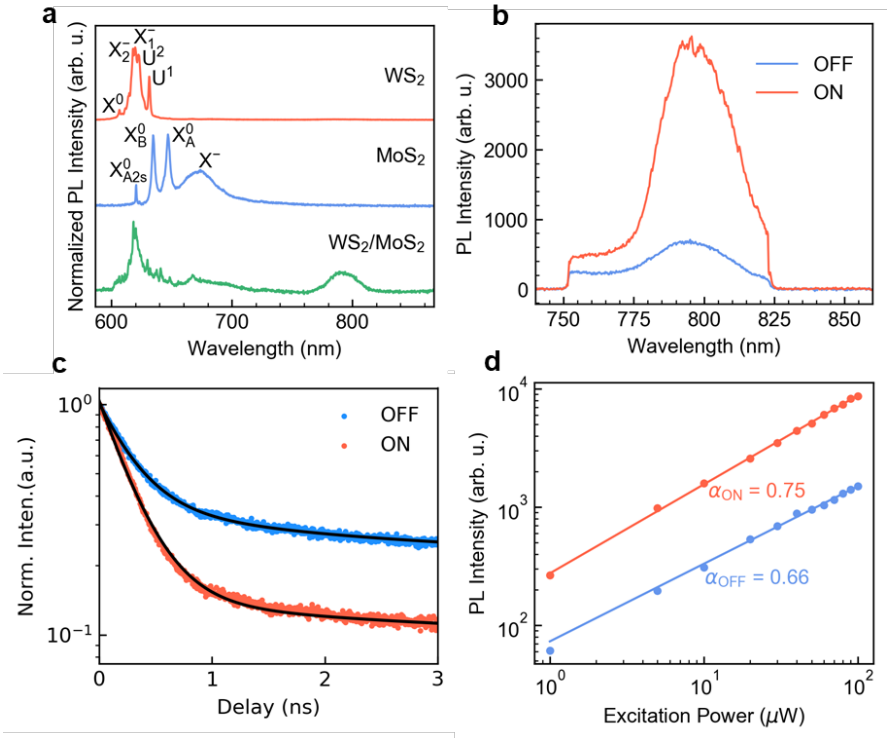

Figure 3. *Plasmonic nanocavity coupling of the interlayer exciton at 5 K. (a) PL spectra of isolated monolayers WS_2(red), MoS_2 (blue) and IEs (green) at 5 K. (b) Interlayer exciton PL comparison between on (red) and off (blue) plasmonic nanocavity. PL intensity increases about 5 times in the coupling region. (c) Time resolved PL shows the reduction in longed-lived IE in both fast and slow decay channels. (d) The PL intensity as the function of excitation power is fitted by a power law (P^{α}) with the critical exponents α.*

We continued to study the system at cryogenic temperatures. The normalised PL spectra at 5K from monolayer WS_2, MoS_2 and IEs are plotted in **Figure 3a**. A narrower excitonic emission from the WS_2 and the MoS_2 monolayers are clearly visible. Comparing the PL emission from IEs on and off cavity, as shown in **Figure 3b**, a 5-time enhancement of the coupled system is observed. **Figure 3c** shows the decay rates of the pristine and cavity coupled IEs emission. The experimental data are fit using a double exponential, with fast / slow decay constants extracted to be 263 ps / 343 ps and 2.29 ns / 3.09 ns for the coupled and non-coupled systems, respectively. The time resolved measurements demonstrate reduction in fast and slow decay channels from IEs to be about 23.3% and 25.8%, respectively. The lifetime reduction at cryogenic temperatures is on part with the change observed at room temperature, consistent with the plasmonic cavities. Finally, **figure 3d** presents the PL intensity of an IE as a function of excitation power for the cavity coupled (red) and pristine system (blue). As expected for the excitonic system, no

saturation is observed.

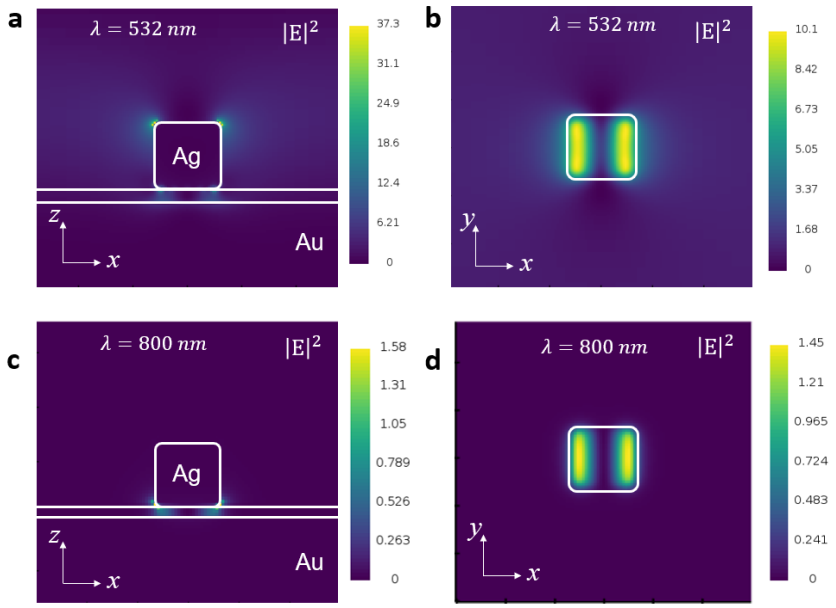

Figure 4. *FDTD simulation results of the gap cavity system. Electric-field mode profiles induced by the out-of-plane dipole source at wavelengths of 532 nm with (a) side and (b) top view. Same model at 800 nm is presented in (c, d).*

To understand the enhancement in more details, we carried out FDTD simulations of the plasmonic cavity system. In the model, we assume a linearly polarized light source with 532 nm is incident from top to bottom, emulating the experimental situation. The sideview (top view) of the mode profiles are depicted in **Figure 4a** (**4b)**, respectively. The excitation enhancement factor is ~ 10 is observed at the mode maximum. To further estimate the enhancement in the radiative decay rates, i.e. Purcell enhancement, an out-of-plane dipole source (λ=800 nm) is placed within the gap. A cross-sectional side and a top view showing the mode induced by the dipole is shown in **Figure 4c** and **4d**, respectively. Note, that these are electric field profiles with dipole emitters with wavelengths of 800 nm. The Purcell factor for the dipole source located at the mode maximum is ~ 200, and calculated using Lumerical by calculating the dipole power with and without a cavity. The dipole power is defined as the amount of power radiated by the dipole at 800 nm.

To quantify the PL enhancement, we define the average PL enhancement factor across a single cavity as: $\langle EF \rangle = (I_{on} \times A_0)/(I_{off} \times A_{cav})$, where Ion is the integrated PL intensity from the IE coupled into the cavity and I_{off} is the PL intensity from IE on bare thermal oxide silicon substrate, A_0 and A_{cav} are the areas of the laser spot and the cavity, respectively. Here we assume that the laser spot is diffraction limited ~$(266nm)^2$ and the cavity size is $(100\ nm)^2$, yielding a maximum <EF> of 106.1 at room temperature and 35.4 and cryogenic temperature, respectively.

To corroborate our experimental results with the simulation values, one can estimate the Purcell enhancement from our experimental data. The small relative lifetime enhancement of 20% at ambient conditions and ~25% at 5K, combined with the simultaneously observed intensity enhancement is indicative that the IEs are dominated by a rather small quantum yield of a few percent, i.e., the experimentally measured lifetime is dominated by non-radiative recombination. For this case, assuming a quantum yield at the range of ~ 0.5 – 2%, the Purcell enhancement is at the range of ~ 12 - 45 in our experiment. Note, that the enhancement measured experimentally corresponds also and to enhancement in the excitation energy as expected for the plasmonic cavity. Note, that this scenario is not unusual, and similar findings are reported for cavity-coupled exciton emission from carbon nanotubes, which display a 20-fold intensity enhancement but only a rather modest lifetime enhancement.

Conclusions

To conclude, we have demonstrated the integration of IEs in MoS_2/WS_2 monolayer heterostructures with plasmonic nanocavities. The IEs interacts with the plasmonic cavity modes, leading to a 15-times enhancement in luminescence at room temperature and a 5-times enhancement in PL intensity at cryogenic temperature, respectively. The enhancement of the emission is attributed to the higher absorption efficiency and the Purcell effect from the cavity. Our findings demonstrate a new method to manipulate the excitonic processes in TMD heterojunctions, which is very important for the design of nanophotonic devices from 2D materials.

Additional Key achievments:

Below we summarize additional key achievements from the project:

- First observation of room temperature magnetic response of quantum emitters in layered material – hexagonal boron nitride (hBN). This was done on in house grown emitters in the red spectral range that makes them promising for quantum sensing (Ref #1)
- Realization of quantum sensing with newly discovered emitters in hBN that possess spin 1. These are the negatively charged boron vacancies. They show strong dependence on magnetic fields, strain and temperature. We also realized coherent control of these emitters. (ref #2,3).
- The challenge with those boron vacancies defects is their dim emission. To address these we coupled them to nanoscale plasmonic and photonic resonators – the first demonstration of vdW spin defects coupled to photonic cavities. (ref #4-6)
- New ways to grow vdW quantum emitters via bottom up processes – specially controlling substrate, emission distribution and growth temperature. This results in a deterministic engineering of emitters with targeted emission wavelengths (ref 7-9). Consequently, these growth methods can be leveraged to grow on waveguides, and create emitter arrays – vital for scalable quantum tech with 2D materials (ref 10-11)
- Ref 13-14 are overarching ***invited*** reviews in the field of nanophotonics with VdW systems, covering engineering, physics and outlook into the future.

List of Publications and Significant Collaborations that resulted from your AOARD supported project

a) papers published in peer-reviewed journals,

1. H. Stern, Q. Gu, J. Jarman, S. Barker, N. Mendelson, D. Chugh, S. Schott, H. Tan, H. Sirringhaus, **I. Aharonovich**, M. Atatüre “Room-temperature optically detected magnetic resonance of single defects in hexagonal boron nitride” nature communications, 13, 618 (2022)
2. A. Gottscholl; M. Diez; V. Soltamov; C. Kasper; D. Krauße; A. Sperlich; M. Kianinia; C. Bradac; **I. Aharonovich**; V. Dyakonov, "Spin defects in hBN as promising temperature, pressure and magnetic field quantum sensors" nature communications 12, 1-8 (2021)
3. A. Gottscholl; M. Diez; V. Soltamov; C. Kasper; A. Sperlich; M. Kianinia; C. Bradac; **I. Aharonovich**; V. Dyakonov, "Room temperature coherent control of spin defects in hexagonal boron nitride" Science Advances 7, eabf3630 (2021)
4. J. E. Fröch; C. Li; Y. Chen; M. Toth; M. Kianinia; S. Kim; I. Aharonovich, "Purcell enhancement of a cavity-coupled emitter in hexagonal boron nitride" Small (2021) in press
5. N. Mendelson; R. Ritika; M. Kianinia; J. Scott; S. Kim; J. E. Fröch; C. Gazzana; M. Westerhausen; L. Xiao; S. S. Mohajerani, S. Strauf, M. Toth, I. Aharonovich, Z.-Q. Xu.

"Coupling Spin Defects in a Layered Material to Nanoscale Plasmonic Cavities" Adv. Mater., 2106046 (2021)

6. J. E. Fröch; L. Spencer; M. Kianinia; D. Totonjian; M. Nguyen; V. Dyakonov; M. Toth; S. Kim; I. Aharonovich, "Coupling spin defects in hexagonal boron nitride to monolithic bullseye cavities" Nano Letters 21, 6549 (2021)
7. Y. Chen; C. Li; S. White; M. Nonahal; Z.-Q. Xu; K. Watanabe; T. Taniguchi; M. Toth; T. T. Tran; **I. Aharonovich**, "Generation of High-Density Quantum Emitters in High-Quality, Exfoliated Hexagonal Boron Nitride" ACS Applied Materials & Interfaces, 13, 47283 (2021)
8. Y. Chen; X. Xu; C. Li; A. Bendavid; M. T. Westerhausen; C. Bradac; M. Toth; I. Aharonovich; T. T. Tran, "Bottom-Up Synthesis of Hexagonal Boron Nitride Nanoparticles with Intensity-Stabilized Quantum Emitters" Small 17, 2008062 (2021)
9. N. Mendelson; L. Morales-Inostroza; C. Li; R. Ritika; M. A. P. Nguyen; J. Loyola-Echeverria; S. Kim; S. Götzinger; M. Toth; I. Aharonovich, "Grain Dependent Growth of Bright Quantum Emitters in Hexagonal Boron Nitride" Adv. Opt. Mater. 9, 2001271 (2021)
10. E. Glushkov; N. Mendelson; A. Chernev; R. Ritika; M. Lihter; R. R. Zamani; J. Comtet; V. Navikas; I. Aharonovich; A. Radenovic, "Direct growth of hexagonal boron nitride on photonic chips for high-throughput characterization" ACS Photonics 8, 2033 (2021)
11. C. Li; N. Mendelson; R. Ritika; Y. Chen; Z.-Q. Xu; M. Toth; I. Aharonovich, "Scalable and Deterministic Fabrication of Quantum Emitter Arrays from Hexagonal Boron Nitride" Nano Lett. 21, 3626-3632 (2021)
12. T. N. Tran; S. Kim; S. J. U. White; M. A. P. Nguyen; L. Xiao; S. Strauf; T. Yang; I. Aharonovich; Z. Q. Xu, "Enhanced Emission from Interlayer Excitons Coupled to Plasmonic Gap Cavities" Small, 2103994 (2021)
13. C. Bradac; Z.-Q. Xu; **I. Aharonovich**, "Quantum energy and charge transfer at two-dimensional interfaces" Nano Lett. 21, 1193-1204 (2021)
14. M Kianinia, ZQ Xu, M Toth, I Aharonovich, “Quantum emitters in 2D materials: Emitter engineering, photophysics, and integration in photonic nanostructures” Applied Physics Reviews 9 (1), 011306

d) *conference presentations without papers Several **invited** and **keynote** talks were presented by Prof Igor Aharonovich as part of the project as detailed below. Title of most talks is “Quantum nanophotonics with hexagonal Boron Nitride”*

1. Korea physics society (2021)	2. IWPSD 2021 keynote
3. MIT QP club	4. SPARC (india) keynote (2022)
5. Metanano – keynote (2021)	6. SECAM workshop on single defects (2022)
7. OSA travel fellow program	8. NOMA (OSA)
9. Argonne national labs	10. MRS spring
11. International Iberian Nanotechnology Laboratory	12. CLEO PR (2022)
13. MRS 2021	

f) *A list any interactions with industry or with Air Force Research Laboratory scientists or significant collaborations that resulted from this work.*

We had several email exchanges with Dr Ruth Patcher but due to covid, travel was not possible.

DD882: There was no IP as a result of the current project. All results were published in the public domain.